CrossMark

X-phase precipitation in aging of Cu–Al–Ni–xTi shape memory alloys and its influence on phase transition behavior

Safaa N. Saud[1] · E. Hamzah[1] · T. Abubakar[1] · H. R. Bakhsheshi-Rad[1] ·
Raheleh Hosseinian[1]

Abstract The present work aims to investigate the aging treatment effects on the microstructure, transition characteristics, and mechanical properties of Cu–Al–Ni–xTi shape memory alloys. The aging treatment of the homogenized and modified alloys of Cu–Al–Ni–xTi results in variations of the martensite morphology, volume fraction, and precipitate size. These variations in the features of precipitates have an obvious effect on transition behavior and mechanical properties. The transition temperatures are increased slightly with an increase in the aging time and temperatures; such increase is mainly attributed to changes in the γ'_1 and β'_1 morphology and distribution, along with the precipitates. The thermodynamic parameters (ΔH and ΔS) tend to decrease with an increase in the aging time and temperatures. Moreover, the brittleness, low strength, and poor processability of Cu–Al–Ni alloys greatly limit their application. We attempted to improve the mechanical properties without losing the thermoelastic properties through the additions of Ti and appropriate aging treatments. The highest tensile strength and strain of 640 MPa and 4.3 % were obtained in alloy of Cu–Al–Ni-0.7 mass% Ti aged at 250 °C for 24 h and 100 °C for 48 h, respectively. The shape memory behavior of the alloys was studied using a specially designed machine. The strain recovery by shape memory effect of the alloys increases with an increase in the aging tomes and temperature, where the highest recovery (100 %) is obtained with the alloy of Cu–Al–Ni-0.7 mass% Ti after being aged at 250 °C for 24 h.

✉ E. Hamzah
  esah@fkm.utm.my

[1] Faculty of Mechanical Engineering, Universiti Teknologi Malaysia (UTM), 81310 Johor Bahru, Johor, Malaysia

Introduction

Shape memory alloys (SMAs) are intelligent materials that can undergo martensitic phase transitions when thermo-mechanical loads are applied, and can recover their original shape when heated above a certain temperature [1, 2]. The shape memory effect (SME) and pseudo-elasticity are the most significant properties that make SMAs remarkably different from other materials [3] that are associated with the way the martensitic transition occurs. During this transition, SMAs transform from the austenite phase, which is usually a cubic lattice structure, to the martensite phase, which has a monoclinic variant lattice structure. The martensitic variants of SMAs are capable of reorienting/detwinning into a single variant by applying mechanical loads, which can result in great inelastic strain [4]. Many alloys exhibit SME and pseudo-elasticity, such as NiTi, Cu-based, and iron-based alloys [5]. As a result of their inexpensive, wide-ranging transition temperatures, as well as their ease of production, their high thermal stability, and small hysteresis with affordable SME, Cu-based SMAs have attracted much attention from scientists and researchers. The binary systems of Cu–Zn and Cu–Al are the main two copper-based alloys that appear in the domains of the β-phase. Among the Cu-based alloys, Cu–Al–Ni SMAs are the most used alloys, particularly whenever high temperatures are required. As such, they are assigned to high transition temperatures that can work at or near 200 °C [6], which is usually difficult for Cu–Zn–Al and NiTi alloys [7, 8], whose maximum temperatures are approximately 100 °C [9]. Under certain conditions, which

depend on thermal and mechanical effects, such as thermal cycling, heat treatment, chemical composition, deformation, an intermediate phases, these alloys may appear between austenite↔martensite transitions, resulting in multi-stages transition. In the Cu–Al–Ni system, M_s temperature has never been lower than 60 °C because of the stability of the aluminum content. An excess of aluminum would induce γ_2 precipitations that lead to the formation of martensite of a 2H microstructure, instead of an 18R microstructure, and causes brittleness and SME deterioration. With nickel addition, while the eutectoid temperature remains at approximately 565 °C, the material experiences eutectoid composition variation that affects the martensite microstructure [10]. Many factors are affected on the transition characteristics of the Cu–Al–Ni SMAs, e.g., adding alloying elements, applying aging treatment, and fabrication techniques [11–15]. Among the aforementioned factors, the aging treatment has been found to be the most significant process for enhancing the shape memory characteristics of the ternary Cu–Al–Ni alloys [11]. The enhancement reason behind the aging treatment is attributed to the formation of precipitates that lead to act as effective obstacles for dislocation movements, thus increasing SME [16]. The size and coherency of the precipitates affect the transition as well as the mechanical strength of the alloy [17]. In an earlier research paper [12], we discussed the effect of Ti additions on the microstructure and mechanical properties of Cu–Al–Ni SMA; thus, the next interesting step is a comprehensive study that investigates the effect of various amounts of aging time and temperature on the phase transition behavior of the modified alloys, as presented in this paper. The temperature range of study was designed based after a preliminary investigation by differential scanning calorimetry (DSC). The results of the current research are expected to provide an understanding of the thermal behavior of Cu-based SMAs with the purpose of obtaining the best control on their performance in applications.

Experimental

The nominal compositions of the alloys were Cu–Al–Ni–xTi SMAs (where x is 0.4, 0.7 and 1.0). The alloys were prepared by an induction furnace using high purity elemental of Cu (99.999 %), Al (99.999 %), Ni (99.995 %) and Ti (99.9 %). These elements were melted in a silicon carbide crucible at a temperature of approximately 1300 °C with continuous stirring and then poured into a cast iron mold with dimensions of $270 \times 50 \times 20$ mm^3. The produced ingots were homogenized at 900 °C for 30 min and then followed by quenching in water to form the martensite phase. Afterward, each ingot was cut in the required dimensions using electrical discharge machining wire

(EDM). Subsequently, the solution-treated samples were aged at temperatures of 100, 150, and 250 °C for 24 and 48 h in the normal atmosphere and then quenched in water. The martensitic transition temperatures were determined by differential scanning calorimetry (Mettler Toledo DSC 822e) in the temperature range of 50–300 °C within the scanning rate of 10 °C min^{-1}. The crystal structure at room temperature (RT) was determined by using D5000 Siemens X-Ray diffractometer fitted with CuKα X-ray source with a locked couple mode, 2θ range between 30–80°, and scanning step 0.05° sec^{-1}. The microstructure morphologies of aged samples were observed by field emission scanning electron microscopy (FESEM) using a Zeiss-LEO Model 1530. Samples for microstructural observation were mechanically polished and etched in a solution consisting of 2.5 g ferric chloride (FeCl$_3$·6H$_2$O) and 48 mL methanol (CH$_3$OH) in 10 mL HCl with concentration of 65 % for 4 min. Tensile stress–strain tests were carried out in according to the E08 standard at a constant head displacement of 0.1 mm min^{-1} using an Instron 5982-type universal testing machine at room temperature, and the gage length of all tensile specimens was 25 mm, as shown in Fig. 1a. Finally, the shape memory effect test was performed using a specially designed machine (Instron 5982-type) operated with special program parameters according to the shape memory test. This machine was connected to a heater tape and digital thermocouple in order to control the applied temperature, and an external extensometer to measure shape extension and recovery. The tests were carried out by loading and unloading the aged sample to a certain strain at a temperature lower than M_f, which was approximately 100 °C. The deformed sample that still had an unrecoverable shape was subsequently heated above the austenite finish temperature, i.e., 300 °C for 10 min, followed by water quench to recover the residual strain (ε_r) [2, 18], as presented in Fig. 1b. The strain recovery ratio was determined as ($\varepsilon_{r-}\varepsilon_p/\varepsilon_p + \varepsilon_r$), whereas ε_p is the plastic strain, and ε_r is the residual strain [19]. The recovered shape was attributed to the transformation of the detwinned martensite to the austenite phase, which had been termed as a transformation strain (ε^t). Subsequent cooling to martensite will again result in the formation of self-accommodated twinned martensitic variants with no associated shape change [4].
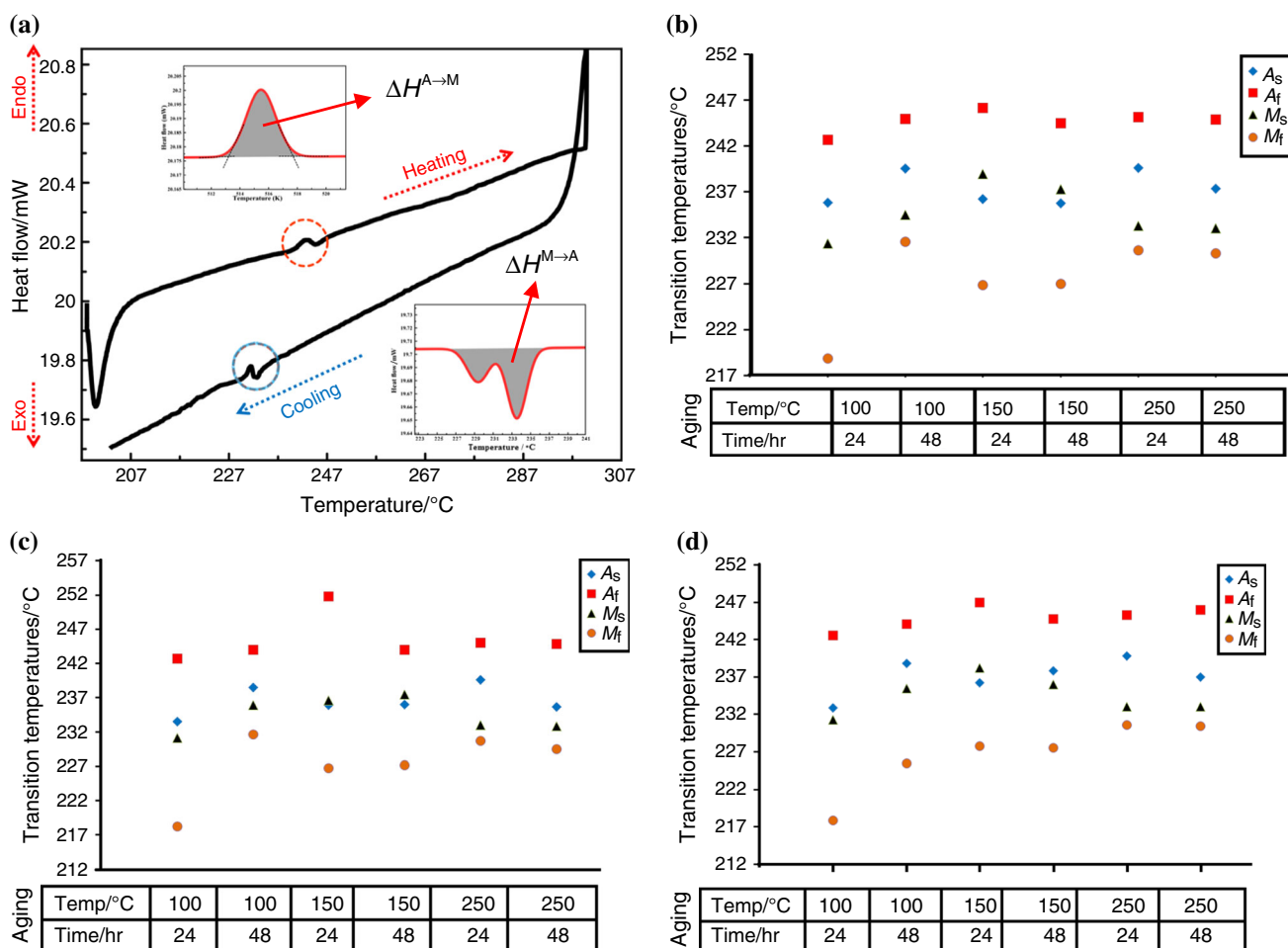
Results and discussion

DSC analysis

The transition curves of the forward and reverse transitions for the Cu–Al–Ni–xTi (x = 0.4, 0.7 and 1.0 mass%) aged at different times and temperatures are illustrated in
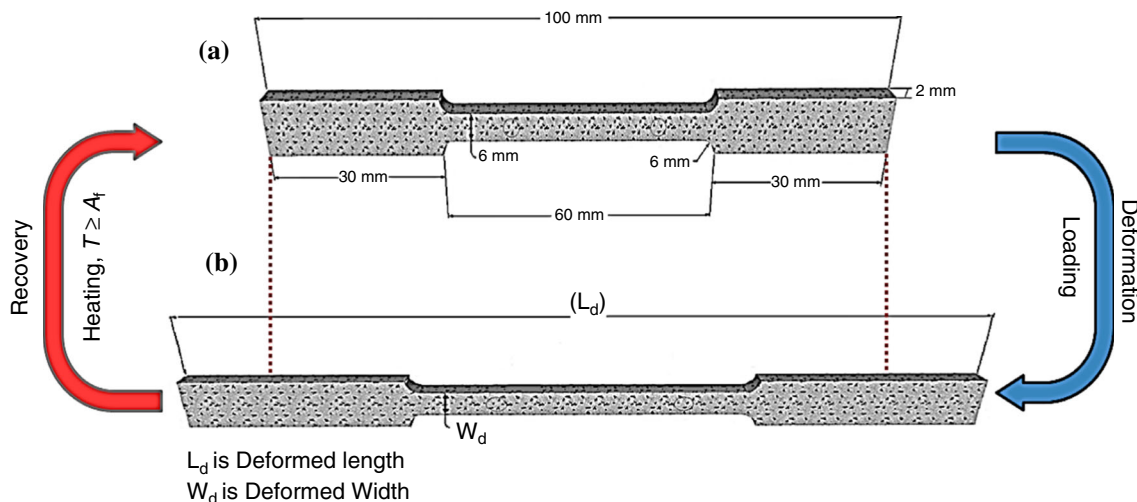
Fig. 1 *a* Schematic of tensile specimen; *b* Schematic of shape memory test includes deformed sample and sample after recovery

Fig. 2 **a** Transition temperature curves for Cu–Al–Ni-0.4 mass% Ti SMA aged at 100 °C for 48 h; transition temperatures for austenite and martensite versus aging time and temperature, **b** Cu–Al–Ni-0.4 mass% Ti SMA, **c** Cu–Al–Ni-0.7 mass% Ti SMA, **d** Cu–Al–Ni-1.0 mass% Ti SMA

Fig. 2a–d. It was found that with an increase in aging time and temperature, the transition temperatures shift toward high temperatures, which is in agreement with other researchers [20–24]. This shifting is mainly attributed to the type and morphology of the martensitic phase, as well as the presence of the precipitates [25, 26]. During the heating and cooling processes, these precipitates hinder the movements of grain interfaces, thus increasing the transition temperatures. As can be observed from Fig. 2a, the cooling curves have multi-peaks, which are attributed to the inner stress and/or precipitate coarsening caused by the inhomogeneity process [27].

The thermodynamic parameters of forward and reverse transition of the aged Cu–Al–Ni–xTi ($x = 0.4$, 0.7 and 1.0 mass%) SMAs were determined and are presented in Fig. 3. The values of the enthalpy were determined in according to the area under the peak of transformation for the endothermic and exothermic curve as shown in Fig. 2a, whereas the entropy values were calculated based on the following relations:

$$\Delta G^{M \to A}(T_o) = G^A(T_o) - G^M(T_o)$$
$$= \left(H^A - T_o S^A\right) - \left(H^M - T_o S^M\right)$$
$$= \Delta H^{M \to A} - T_o \Delta S^{M \to A} \quad (1)$$

Or

$$\Delta G^{A \to M}(T_o) = G^M(T_o) - G^A(T_o)$$
$$= \left(H^M - T_o S^M\right) - \left(H^A - T_o S^A\right)$$
$$= \Delta H^{A \to M} - T_o \Delta S^{A \to M} \quad (2)$$

for the alloy, when the $\Delta G^{M \to A}(T_o)$ and $\Delta G^{A \to M}(T_o) = 0$ at $T = T_o$ is expressed as [28, 29]:

$$T_o = \frac{\Delta H^{MA}}{\Delta S^{MA}} \text{ or } T_o = \frac{\Delta H^{AM}}{\Delta S^{AM}} \quad (3)$$

The equilibrium temperature between the austenite and martensite phase transition can be expressed as follows:

$$T_o = \frac{1}{2}(M_s + A_f) \quad (4)$$

The enthalpy (ΔH) and entropy (ΔS) of both transitions varied with different aging time and temperature. Because an inverse proportional relationship exists between thermal stability and enthalpy, it was found that the aged alloy of 150 °C for 24 h for the 0.4 mass% Ti, 0.7 mass% Ti, and 100 °C for 24 h for 1.0 mass% Ti addition aged alloys obtained the highest martensite thermal stability, which may relate to the amount of precipitates, behavior, and morphology of the martensite phase.
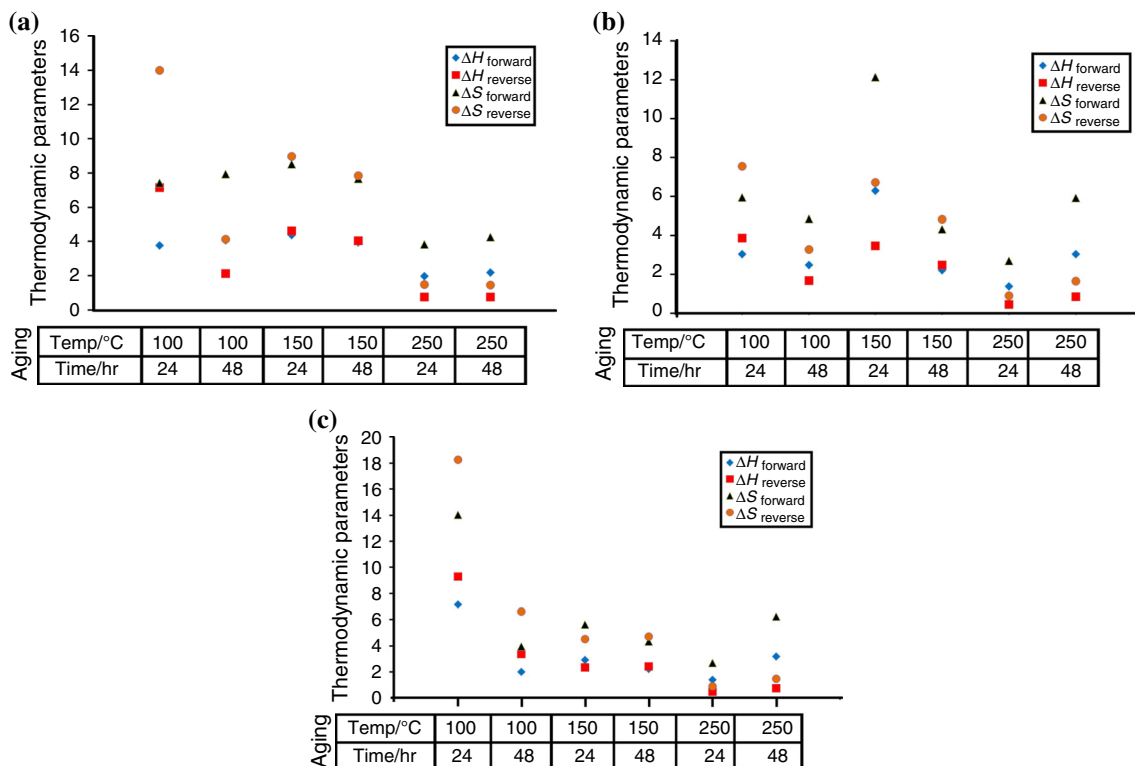
Fig. 3 Enthalpy and entropy of the forward and reserve transitions versus aging time and temperature: a Cu–Al–Ni-0.4 mass% Ti SMA, b Cu–Al–Ni-0.7 mass% Ti SMA, c Cu–Al–Ni-1.0 mass% Ti SMA

Microstructural characteristics

The microstructures of the aged Cu–Al–Ni–xTi are shown in Figs. 4a–i and 5a–i. It is apparent that the aged microstructures obtained the same phases of the un-aged alloys [12] γ'_1 and β'_1, along with the precipitates. However, the microstructures changed in terms of morphologies, orientations, and volume fractions. These differences are mainly related to the phenomena of every aging condition. For instance, at 0.4 mass% Ti aged alloys, it is found that the thickness of γ'_1 plate-like decreases gradually with an increase in the aging times and temperatures, linked to an increase in the volume fraction and thickness of β'_1 needle-like. Furthermore, the volume fractions of the acquired precipitates also increase with further aging time and temperature. Nevertheless, with the aging treatment, these types of precipitates are penetrated into the plate-like and needle-like, as shown in Figs. 4a, d, g and 5a, d, g. At 0.7 mass% Ti aged alloys, the microstructures are formed by a thick sharp needle-like categorized on β'_1 phase, and the majority of the area is covered by a group of γ'_1 plate-like, as shown in Figs. 4b, e, h and 5b, e, h, which belongs to a self-accommodation group of multi-variants along

with an irregular flower shape that belongs to the X-phase [8]. After the aging treatment, the precipitates are accommodated at the grain boundaries, particularly, at 100 °C for 24 and 48 h. These types of precipitates return to the consistent flower of the 0.4 Ti, as shown in Figs. 4a and 5a. This means that the precipitates formed on the plate-like and needle-like, and their volume fraction was reduced in association with increases in size. On the other hand, with 250 °C as the aging temperature for 24 and 48 h, the volume fraction of precipitates increased as shown in Figs. 4g and 5g. However, when the aging time and temperature increases, the β'_1 needle-like and γ'_1 plate-like usually vary in terms of volume fraction, size, and morphology. The aged 1.0 Ti mass% addition microstructures display a similar behavior as 0.7 Ti aged alloys, as shown in Figs. 4c, f, i and 5c, f, i.

At 100 °C aging temperatures for 24 h, the volume fraction for both X-phase and β'_1 phases decreases, whereas the thickness and volume fraction of γ'_1 phase increases. The precipitates are also penetrated into the needle-like and plate-like, as shown in Fig. 4c. Nevertheless, at the aging temperature of 100 °C for 48 h, the shapes associated with these precipitates are transformed to
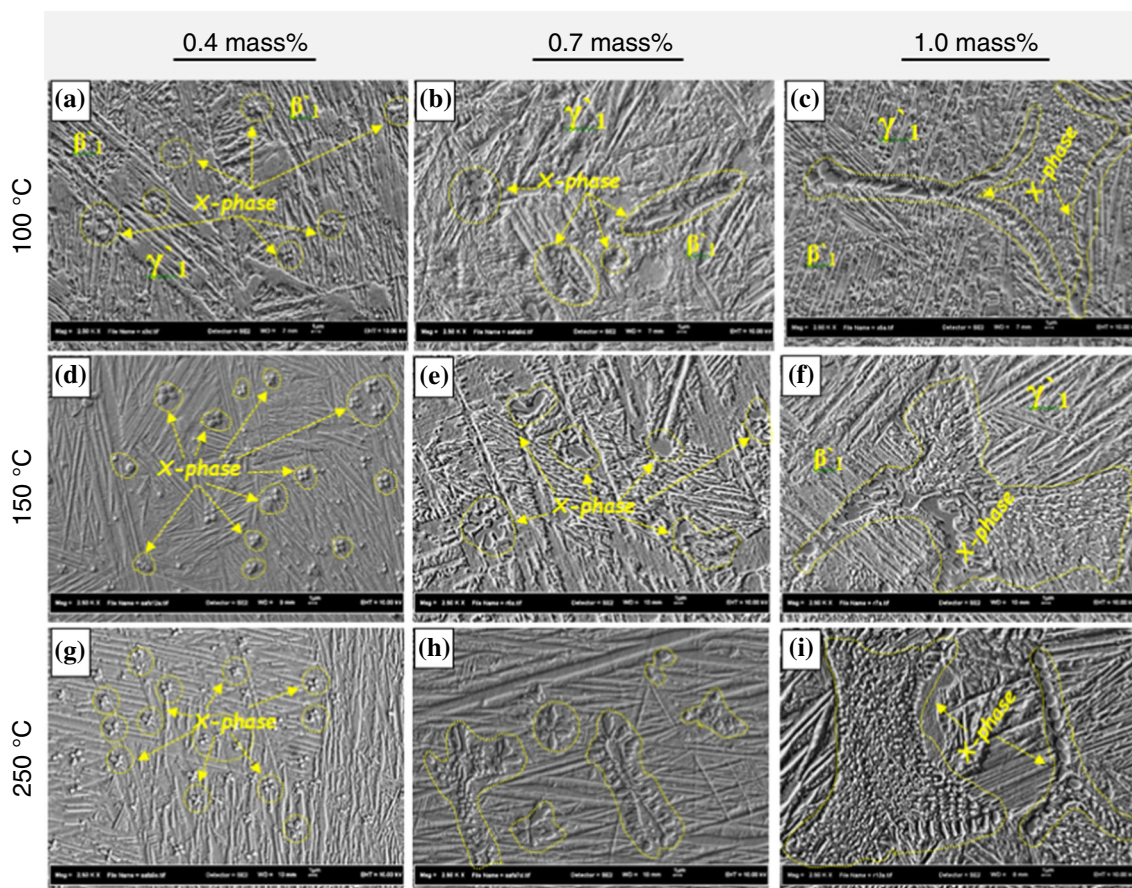
Fig. 4 FESEM micrographs of the microstructures for Cu–Al–Ni–xTi SMA (x = 0.4, 0.7 and 1.0 mass%) at 24 h aging time
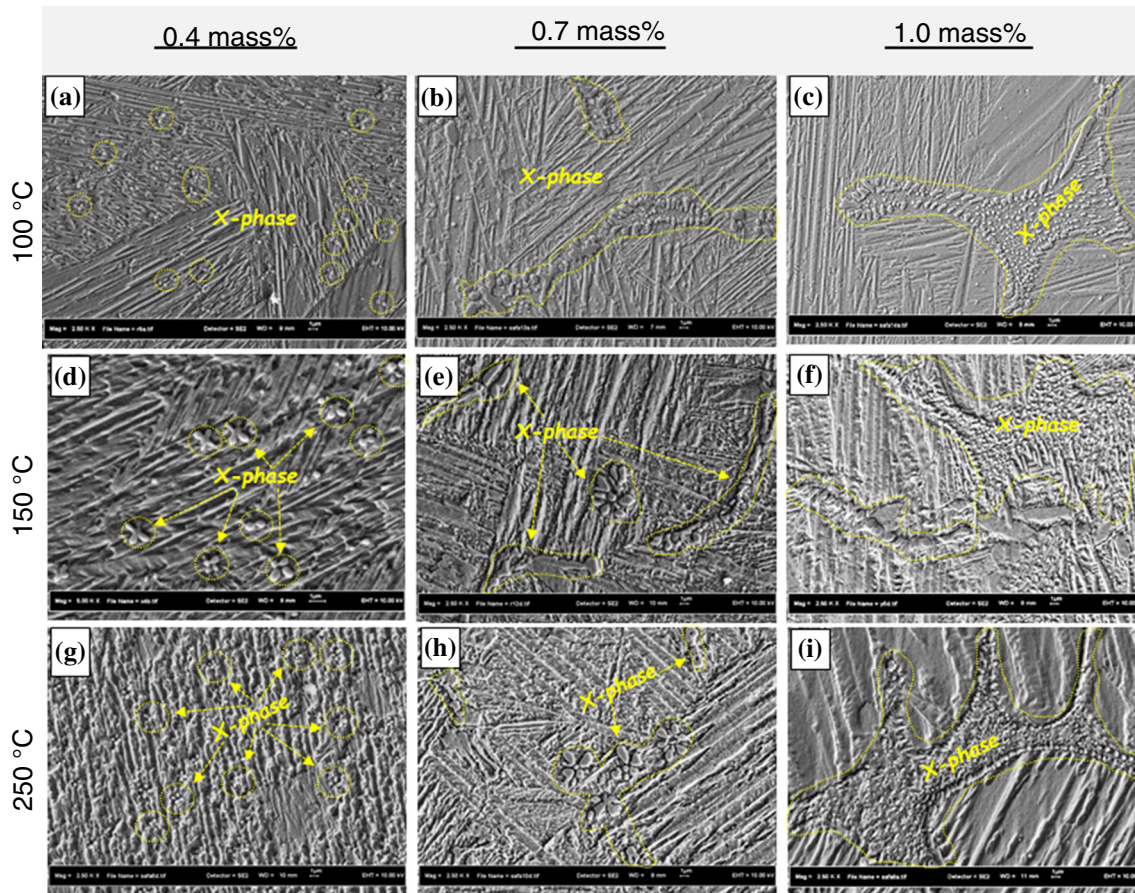
Fig. 5 FESEM micrographs of the microstructures for Cu–Al–Ni–xTi SMA (x = 0.4, 0.7 and 1.0 mass%) at 48 h aging time

be irregular along with the variety in size of precipitates, as shown in Fig. 5c. According to this findings, the incomplete transition of austenite to martensite of the X-phase and β'_1 phases demonstrate an increase in volume fraction. The γ'_1 phase grows in a V-shape, and the area between these plate-like is filled by a needle-like of the β'_1 phase. With a further increase in the aging time and temperature, the precipitates begin to move and grow around the grain boundaries, forming an ellipse shape, which starts with a small size at 24 h and grows with 48 h aging time as shown in Figs. 4f and 5f. Simultaneously, the γ'_1 and β'_1 phases show the same behavior of the aged Cu–Al–Ni-0.7 mass% Ti SMA. When the aging temperature increases to 250 °C for 24 h, the X-phase precipitates disperse and penetrate the needle-like and plate-like, as shown in Fig. 4i. With further increase in the aging time to 48 h, the precipitates move to surround the grain boundaries with a different size of spherical shape. The plate thicknesses of the γ'_1 phase increases in correlation with a decrease in the volume fraction of the β'_1 phase, as shown in Fig. 5i.

Figure 6a–c displays the XRD of the aged alloys for 0.4, 0.7 and 1.0 mass% Ti additions, respectively. It can be noticed that the XRD patterns of the aged samples show almost the same patterns in the un-aged samples (as mentioned in the previous paper of this research [12]) that can confirm the presence of the same phases in the microstructures of the aged samples. The only difference is that after the aging treatment, a slight shifting occurs that is associated with variations in the values of intensity. However, the X-phase is verified by the existence of three compounds in the form of single compound or multi-compounds. The volume fraction of the X-phase can also be confirmed via the intensity of the XRD patterns. As can be seen, the intensities for the precipitate pattern peaks change in accordance with the volume fraction of the X-phase.

On the other hand, the lattice parameters were determined and are tabulated in Table 1. The determination was conducted based on the monoclinic structure, and using the following relationship [30]:

$$\frac{1}{d^2} = \frac{1}{a^2}\left[\frac{h^2}{\sin^2\beta}\right] + \frac{k^2}{b^2} + \frac{1}{c^2} + \left[\frac{l^2}{\sin^2\beta}\right] - \frac{2hl\,\cos\beta}{ac\,\sin^2\beta} \quad (5)$$

where d is the spacing distance; a, b and c are the lattice parameters and (hkl) Miller indices; and β is the angle. Based on the XRD patterns displayed in Fig. 6, it is found

(a)

(b)

(c)
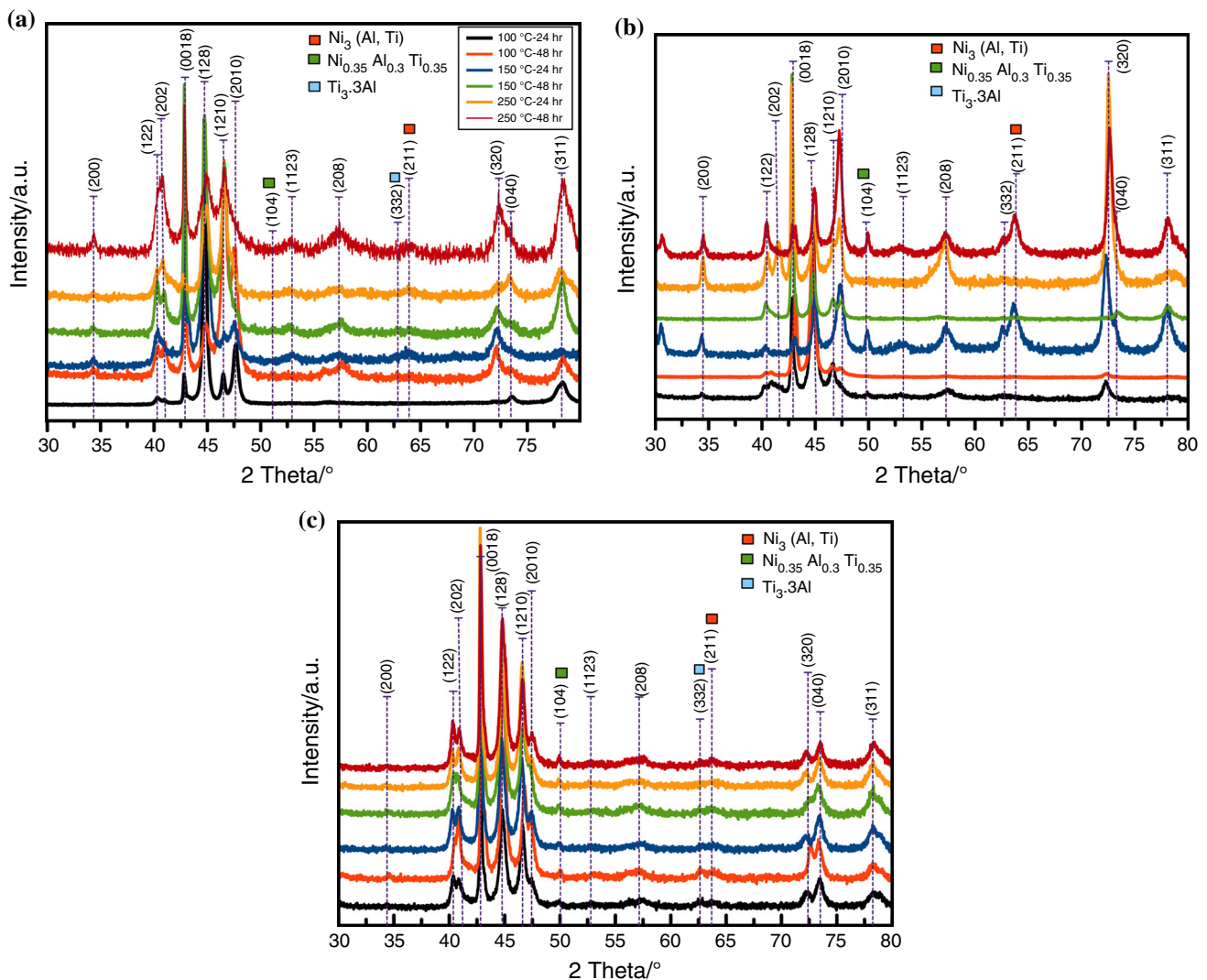
Fig. 6 XRD patterns for: **a** Cu–Al–Ni-0.4 mass% Ti SMA, **b** Cu–Al–Ni-0.7 mass% Ti SMA, **c** Cu–Al–Ni-1.0 mass% Ti SMA

that the lattice parameters change because of the variations of aging time and temperature. It is also found that the highest lattice parameters are indicated with the aged alloy of 1.0 mass% Ti addition.

Mechanical properties

Tensile tests

Figure 7a–c displays the stress–strain curves of the Cu–Al–Ni–xTi (x = 0.4, 0.7 and 1.0 mass%) at room temperature. It can be observed that the response of the stress–strain performance changes significantly with the aging treatment conditions. The aging alloy at 100 °C for 48 h demonstrated higher ductility for the 0.4 and 0.7 mass% Ti compared with other alloys, as shown in Fig. 7a, b. However, the 1.0 mass% exhibits the highest ductility at 150 °C for

24 h, as shown in Fig. 7c. The highest stress is 485, 640, and 635 MPa attained with aging at 150 °C for 48 h for 0.4 mass%, 250 °C for 24 h for 0.7 mass%, and 150 °C for 24 h, respectively. These types of improvements are caused by the volume fraction of the precipitates and β'_1 phase; on the other hand, both can restrict the mobility of the dislocations and grain interfaces, and reducing their mobility can serve to increase strength. Other researchers reported that the formation of Ti-rich precipitates in the strain of Cu–Al–Ni SMA can result in improving the stress–strain curve response [31], and thereby, the mechanical properties are enhanced to owning this alloy. The results of the fracture stress and strain are listed in Table 2.

Meanwhile, Khan and Delaey [32] reported that the grain size has an effect on the tensile properties, having found that a smaller grain size can certainly increase the fracture stress and strain with respect to the Hall–Patch

Table 1 Lattice parameters for Cu–Al–Ni–xTi SMA under different aging conditions

| Alloy	Aging		Lattice parameters			
	Temperature	Time	a/Å	b/Å	c/Å	β
Cu–Al–Ni-0.4 mass% Ti	100 °C	24 h	3.97	5.11	38.89	76.16
	100 °C	48 h	4.05	5.69	41.56	94.14
	150 °C	24 h	4.10	5.22	41.17	80.68
	150 °C	48 h	4.46	6.45	52.12	117.60
	250 °C	24 h	3.67	5.24	38.37	90.49
	250 °C	48 h	4.16	5.18	39.22	82
Cu–Al–Ni-0.7 mass% Ti	100 °C	24 h	4.08	6.01	45.45	103
	100 °C	48 h	4.10	5.77	38.17	96.32
	150 °C	24 h	3.78	6.31	43.90	97.30
	150 °C	48 h	3.86	5.25	38.82	90.93
	250 °C	24 h	4	5.62	38.52	94.35
	250 °C	48 h	3.77	6.29	44.09	97.35
Cu–Al–Ni-1.0 mass% Ti	100 °C	24 h	4.92	5.43	48.96	126.42
	100 °C	48 h	4.31	5.38	49.71	111.59
	150 °C	24 h	4.90	5.42	48.53	125.89
	150 °C	48 h	4.12	5.29	38.72	95.34
	250 °C	24 h	3.52	5.26	38.80	87.13
	250 °C	48 h	4.63	5.84	41.14	111.72

relationship ($\sigma_y = \sigma_o + K_y/\sqrt{d}$). The behavior of stress–strain for the entire Ti addition aged alloys revealed two obvious regions during loading. The first region is a non-linear elastic stage that represents the multi-variants martensite reorientations. As a result of the presence of the precipitates that may lead to incompletion of the martensite reorientations, higher stress would be necessary. The second region represents the reorientations of martensite along with some deformation of martensite–martensite-induced transition, in which this region increases with a near-linear relationship, and the bending area obtained that is blocked to the fracture region refers to the further martensite–martensite transition.

The fracture surface areas of the tensile specimens of the aged 0.4 mass% Ti addition samples are presented in Fig. 7aI–aVI. Typically, the aged alloys demonstrate a different type of fracture characteristic in accordance with the applied aging time and temperature. Figure 7aI reveals an inter-granular fracture that is indicated by improvement in ductility in a stress–strain curve. By way of increasing the aging time to 48 h at the same aging temperature of 100 °C, brittle fracturing decreases. On the other hand, the fracture surface of this alloy demonstrates a mixed feature of quasi-cleavage with a tearing ridge, as well as some of the ductile dimples, as shown in Fig. 7aII, which is in agreement with the increment of ductility of this alloy in Fig. 7a. Nevertheless, the increase in the aging temperature to 150 °C for 24 h characteristically displays a trans-granular with slight area of the ductile dimples, as shown in Fig. 7aIII that can imply a ductile fracture. Figure 7aIV exhibits a quasi-cleavage feature that presents a brittle fracture. Furthermore, the 250 °C for 24 h alloy aging indicates a mixed mode of quasi-cleavage with a ductile dimple rupture, as shown in Fig. 7aV, which is in complete agreement with the behavior of the stress–strain curve shown in Fig. 7a. When the aging time increases to 48 h at an aging temperature of 250 °C, the cleavage area is reduced and changes to a typically ductile dimple area, which could refer to the ductile fracture shown in Fig. 7aVI.

The aged alloys of the 0.7 mass% Ti addition display the same variety of fracture features as the aged 0.4 mass% Ti addition, as shown in Fig. 7bI–bVI. It is found that in the aging treatment of 100 °C for 24 h alloy, the fracture surface indicates a mixed mode of trans-granular and inter-granular features, as shown in Fig. 7bI, which can refer to a particularly brittle fracture. Figure 7bII shows an enlarged area of ductile dimples that reflect a ductile fracture. With an increase in the aging temperature to 150 °C for 24 h, the fracture feature transfers to a trans-granular fracture, as shown in Fig. 7bIII. This occurs despite the fact that with 150 °C for 48 h alloy, the fracture surfaces are covered with ductile dimples that lead to a substantial number of secondary cracks, as shown in Fig. 7bIV. The signs that remain on the fracture surface by two large removed plate-like are also apparent on the sides of this micrograph. The
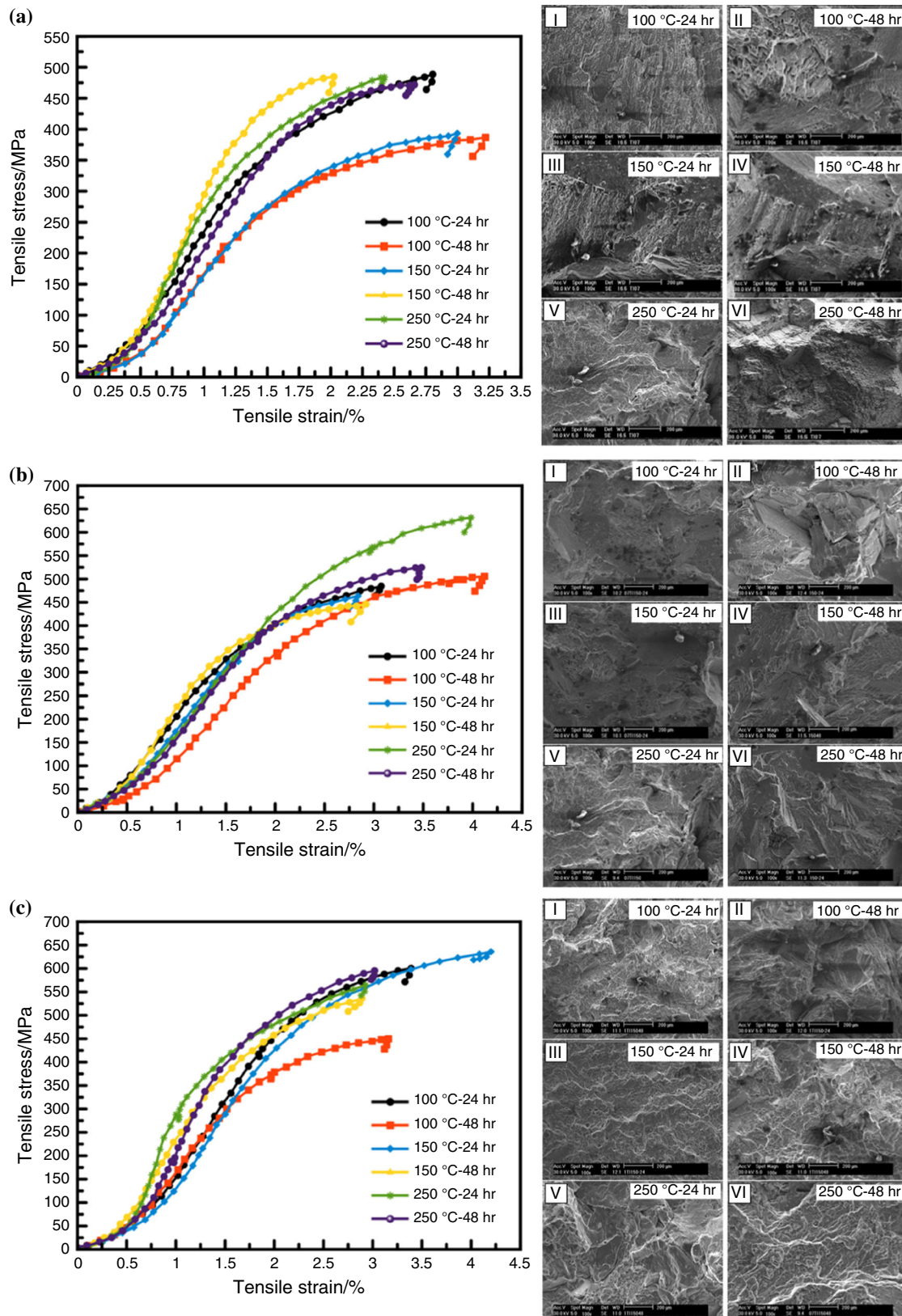
Fig. 7 Tensile stress–strain curves for SMA: **a** Cu–Al–Ni-0.4 mass% Ti, **b** Cu–Al–Ni-0.7 mass% Ti, **c** Cu–Al–Ni-1.0 mass% Ti

Table 2 Fracture stress–strain and strain recovery ratio for aged Cu–Al–Ni–xTi SMA at different aging conditions

Alloy	Aging		Properties		
	Temperature/ °C	Time/ h	Fracture stress (σ^F)/MPa	Fracture strain (ε^F)/%	Strain recovery ratio by SME (ε_{SME})/%
Cu–Al–Ni-0.4 mass% Ti	100	24	480	2.86	54
	100	48	380	3.2	58
	150	24	390	3	70
	150	48	485	2	90
	250	24	480	2.4	80
	250	48	470	2.65	77
Cu–Al–Ni-0.7 mass% Ti	100	24	480	3.2	80
	100	48	510	4.2	87
	150	24	470	2.8	82
	150	48	450	2.9	81
	250	24	640	4	100
	250	48	525	3.5	70
Cu–Al–Ni-1.0 mass% Ti	100	24	600	3.4	68
	100	48	450	3.2	70
	150	24	635	4.2	80
	150	48	540	2.85	77
	250	24	565	2.9	85
	250	48	600	3	98

fractographic examination of 250 °C for 24 and 48 h alloys reveal an inter-granular characteristic along with large ductile dimples, as shown in Fig. 7bV, bVI, which can conveniently clarify the behavior of the stress–strain curves of these alloys, as shown in Fig. 7b. Overall, the results show that when the Cu–Al–Ni alloy is modified by the addition of alloying elements and application of the aging treatment, ductility is improved as indicated by the values of elongation to fracture. For the fractured surfaces of 1.0 mass% Ti addition aged alloys, the surface fractures show inter-granular features along with some dimple ruptures for the first four alloys, which are 100 °C for 24 h, 100 °C for 48 h, 150 °C for 24 h, and 150 °C for 24 h, as presented in Fig. 7cI–cIV. The alloys of 250 °C for 24 h and 48 h show a mixed mode feature between an inter-granular and some quasi-cleavage areas, as indicated in Fig. 7cV–cVI.

Shape memory effect test

Figure 8a–c shows the strain recovery ratio of the Cu–Al–Ni–xTi (x = 0.4, 0.7 and 1.0 mass% Ti), respectively, under different aging times and temperatures. The study found that the variations of the aging conditions have a significant influence on SME by reversing the existing martensite and changing the microstructure of the martensite parent phase, in particular, the structure of

stacking faults and dislocations caused by the presence of precipitates into the microstructure of these alloys. In addition, their volume fraction depends mainly on the condition of aging treatment, and the shape memory characteristics vary in terms of the strain recovery ratio caused by SME and the recovery ratio [33, 34]. Figure 8a shows the shape recovery of the 0.4 mass% Ti addition aged alloys, and the determined data are recorded in Table 2. This study establishes that the highest shape recovery is obtained when the modified alloy is aged at 150 °C for 48 h, which exhibits 90 % shape recovery of the original shape after being heated to a temperature higher than A_f; 300 °C. Figure 8b shows SME for the 0.7 mass% Ti addition aged alloys, and the recorded data are shown in Table 2. It is noticed that these alloys obtained similar shape recovery behavior to the 0.4 mass% Ti addition aged alloys. When the alloy is aged at 250 °C for 24 h, the SME abruptly increases, which exhibits complete recovery of the original shape after being heated higher than the A_f; at 300 °C. This increment in shape recovery is related to the enhancement of the yield strength of this alloy after being aged. The yield strength is associated with the reorientation of martensitic variants and/or detwinning [35]. On the other hand, the formation of (Ni$_3$(Al, Ti), Ti$_3$·3Al, and Ni$_{0.35}$Al$_{0.3}$Ti$_{0.35}$) precipitates, along with increased volume fraction and the needle-like size of the β'_1 phase, can
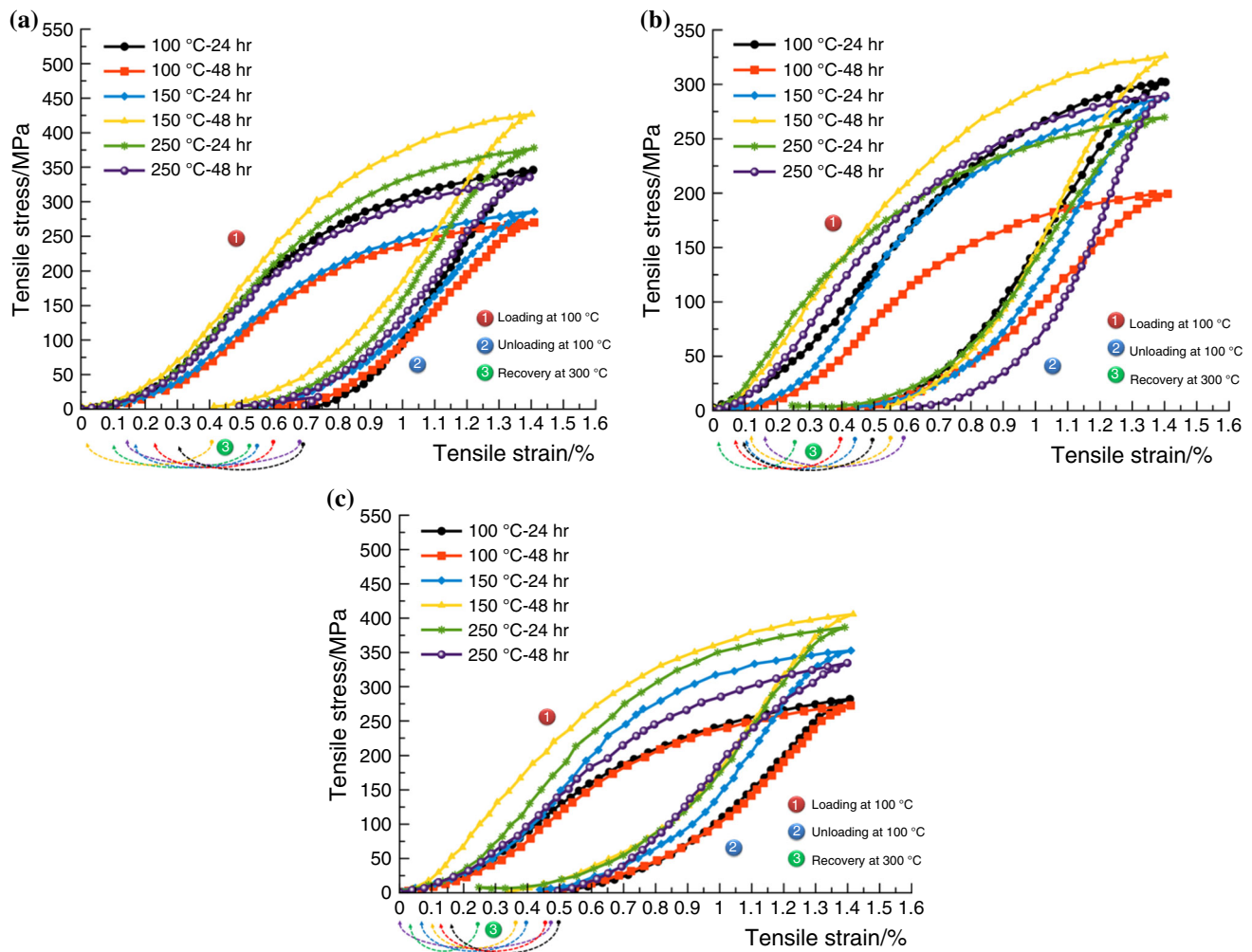
Fig. 8 SME curves for the aged: **a** Cu–Al–Ni-0.4 mass% Ti, **b** Cu–Al–Ni-0.7 mass% Ti, **c** Cu–Al–Ni-1.0 mass% Ti

effectively hinder plastic deformation and increase strength, thus increasing SME.

Figure 8c shows SME for the 1.0 mass% Ti addition aged alloys, and the recorded data are shown in Table 2. It is found that 1.0 mass% Ti addition aged alloys exhibit the highest shape recovery with the 250 °C for 48 h alloy, which obtains a 98 % shape recovery compared with other alloys. Furthermore, it is noticed that shape recovery increases gradually with an increase in the aging time and temperature of this alloy. The SME variations are attributed to two main aspects [36]: the first is the presence of the precipitates along with an increase in the volume fraction of the β'_1 needle-like phase that leads to formation into the microstructure and restricts the mobility of dislocations and boundary interfaces, thus increasing the yield strength of the alloy associated with SME increases [37, 38]. The second aspect is the grain refinement that leads to enhancement in the strength of the alloys, and thus the strain of the permanent slipping is decreased [38]. This factor is directly proportional with SME.

Conclusions

The influences of different conditions of aging treatments on the transition characteristics and mechanical properties of Cu–Al–Ni–xTi SMAs were investigated, and the results observed are as follows:

1. The transition temperatures of the austenite↔martensite phase increased slightly with an increase in the aging time and temperatures. Evaluation of the transition temperatures were influenced by the formation of precipitates that led to hindering the movements of grain interfaces, and thus increased the transition temperatures. The aging treatment caused a decrease in thermodynamics parameters, i.e., enthalpy and entropy.

2. Observations showed that the β_1' and γ_1' martensite phases coexist, but at different volume fractions in the aged alloys. The aging-induced martensites formed as a new phase known as the X-phase, and the percentage

of this phase varied according to the applied aging time and temperature. Increasing the aging temperature caused an increase in volume fraction of the X-phase. However, the shapes of these precipitates changed from regular flower to irregular as a result of aging.

3. With aging, the evolution of the X-phase, including the volume fraction, distribution, and size, was significantly affected by the tensile properties, SME, and fracture behavior. The tensile strength, ductility, and SME of Cu–Al–Ni–xTi SMAs varied according to aging time and temperature, where the highest values of 640 MPa, 4.2 and 100 % recovery were obtained with the alloy of 0.7 w% Ti after being aged at 250 °C for 24 h and 100 °C for 48 h, respectively. The alloy exhibited different fracture features, which varied between inter-granular, quasi-cleavage, and ductile types. These changes are mainly attributed to the occurrence of precipitations and the variation of the γ'_1 and β'_1 morphology.

References

1. Gandhi V, Thompson BS. Smart materials and structures. London: Springer; 1992.

2. Otsuka K, Wayman CM. Shape memory materials. Reprint, illustrated ed. Cambridge: Cambridge University Press; 1999.

3. Vokoun D, Kafka V, Mesomechanical modeling of shape memory effect. In: Symposium on smart structures and materials: International Society for Optics and Photonics; 1999

4. Kumar P, Lagoudas D. Introduction to shape memory alloys. Berlin: Springer; 2008.

5. Nishiyama Z, Fine ME, Wayman CM. Martensitic transformation. London: Academic Press; 1978.

6. Ibarra A, Juan JS, Bocanegra EH, Nó ML. Thermo-mechanical characterization of Cu–Al–Ni shape memory alloys elaborated by powder metallurgy. Mater Sci Eng A. 2006;438–440:782–6.

7. Recarte V, Pérez-Landazábal JI, Nó ML, San Juan J. Study by resonant ultrasound spectroscopy of the elastic constants of the β phase in Cu–Al–Ni shape memory alloys. Mater Sci Eng A. 2004;370(1–2):488–91. doi:10.1016/j.msea.2003.06.004.

8. Font J, Cesari E, Muntasell J, Pons J. Thermomechanical cycling in Cu–Al–Ni-based melt-spun shape-memory ribbons. Mater Sci Eng A. 2003;354(1–2):207–11.

9. Pérez-Landazábal JI, Recarte V, Sánchez-Alarcos V, Nó ML, Juan JS. Study of the stability and decomposition process of the β phase in Cu–Al–Ni shape memory alloys. Mater Sci Eng A. 2006;438–440:734–7. doi:10.1016/j.msea.2005.12.066.

10. Mukunthan K, Brown L. Preparation and properties of fine grain β-CuAlNi strain-memory alloys. Metall Trans A. 1988;19(12):2921–9.

11. Saud S, Hamzah E, Abubakar T, Bakhsheshi-Rad HR. Thermal aging behavior in Cu–Al–Ni–xCo shape memory alloys. J Therm Anal Calorim. 2015;119(2):1273.

12. Saud S, Hamzah E, Abubakar T, Zamri M, Tanemura M. Influence of Ti additions on the martensitic phase transformation and mechanical properties of Cu–Al–Ni shape memory alloys. J Therm Anal Calorim. 2014;118(1):111–22.

13. Saud S, Hamzah E, Abubakar T, Bakhsheshi-Rad HR, Zamri M, Tanemura M. Effects of Mn additions on the structure, mechanical properties, and corrosion behavior of Cu–Al–Ni shape memory alloys. J Mater Eng Perform. 2014;23(10):3620–29.

14. Yildiz K, Kok M. Study of martensite transformation and microstructural evolution of Cu–Al–Ni–Fe shape memory alloys. J Therm Anal Calorim. 2014;115(2):1509–14.

15. Balo ŞN, Sel N. Effects of thermal aging on transformation temperatures and some physical parameters of Cu–13.5 wt%Al–4 wt%Ni shape memory alloy. Thermochim Acta. 2012;536:1–5.

16. Sobrero CE, La Roca P, Roatta A, Bolmaro RE, Malarría J. Shape memory properties of highly textured Cu–Al–Ni–(Ti) alloys. Mater Sci Eng A. 2012;536:207–15.

17. Sinha A, Mondal B, Chattopadhyay PP. Mechanical properties of Ti–($\sim$49 at%) Ni shape memory alloy, part II: effect of ageing treatment. Mater Sci Eng A. 2013;561:344–51.

18. Lagoudas DC. Shape memory alloys: modeling and engineering applications. Berlin: Springer; 2008.

19. Imran Khan M, Kim HY, T-h Nam, Miyazaki S. Formation of nanoscaled precipitates and their effects on the high-temperature shape-memory characteristics of a $Ti_{50}Ni_{15}Pd_{25}Cu_{10}$ alloy. Acta Mater. 2012;60(16):5900–13.

20. Picornell C, Pons J, Cesari E. Effects of thermal ageing in β-phase in Cu–Al–Ni single crystals. J Phys IV. 1997;7(C5):C5-323-C5-8.

21. Zarubova N, Gemperle A, Novak V. Initial stages of γ_2 precipitation in an aged Cu–Al–Ni shape memory alloy. Mater Sci Eng A. 1997;222(2):166–74.

22. Zarubova N, Gemperle A, Novak V. Ageing Phenornena in a Cu–Al–Ni Alloy. J Phys IV. 1997;7(C5):C5-281-C5-6.

23. Guenin P. Thermal aging behaviour and origin of a Cu–Al–Ni shape memory alloy. Mater Sci Eng A. 1990;129:273–7.

24. Daricek T, Lasek J, Zarubova N, Novak V, Bartuska P. Ageing effects in a Cu–Al–Ni shape memory alloy. J Phys IV. 2001;11(PR8):Pr8-179-Pr8-84.

25. Tarhan EF. Aging characteristics of copper based shape memory alloys. Middle East Technical University; 2004.

26. Bouabdallah M, Baguenane-Benalia G, Saadi A, Cheniti H, Gachon J-C, Patoor E. Precipitation sequence during ageing in β1 phase of Cu–Al–Ni shape memory alloy. J Therm Anal Calorim. 2013;112(1):279–83.

27. Suresh N, Ramamurty U. Aging response and its effect on the functional properties of Cu–Al–Ni shape memory alloys. J Alloy Compd. 2008;449(1–2):113–8.

28. Tatar C. Gamma irradiation-induced evolution of the transformation temperatures and thermodynamic parameters in a CuZnAl shape memory alloy. Thermochim Acta. 2005;437:121–5.

29. Ortín J, Planes A. Thermodynamics of thermoelastic martensitic transformations. Acta Metall. 1989;37(5):1433–41.

30. Xuan Q, Bohong J, Hsu TY. The effect of martensite ordering on shape memory effect in a copper–zinc–aluminium alloy. Mater Sci Eng. 1987;93:205–11.

31. Roh DW, Kim JW, Cho TJ, Kim YG. Tensile properties and microstructure of microalloyed Cu-A1-Ni-X shape memory alloys. Mater Sci Eng A. 1991;136:17–23.

32. Khan A, Delaey L. The effect of grain size on the strength of Cu–Al Beta'-martensite. Z Metallkd. 1969;60(12):949–51.

33. Dogan E. CoNiGa high temperature shape memory alloys. Texas A&M University; 2010.

34. Otsuka K, Ren X. Recent developments in the research of shape memory alloys. Intermetallics. 1999;7(5):511–28.

35. Ma Y, Yang S, Wang C, Liu X. Tensile characteristics and shape memory effect of Ni56Mn21Co4Ga19 high-temperature shape memory alloy. Scripta Mater. 2008;58(10):918–21.

36. Yang JP, Kim YG. Tensile properties and shape memory effect of chromium-varied Fe30Mn5SiCr shape memory alloys. Mater Sci Eng A. 1992;154(1):L1–3.

37. Duerig T, Pelton A. Ti-Ni shape memory alloys. In: Boyer R, Collings EW, Welsch G, editors. Materials properties handbook: titanium alloys. USA: ASM International; 1994. pp. 1035–48.

38. Ma Y, Yang S, Liu Y, Liu X. The ductility and shape-memory properties of Ni–Mn–Co–Ga high-temperature shape-memory alloys. Acta Mater. 2009;57(11):3232–41.